Metallomics

Accepted Manuscript

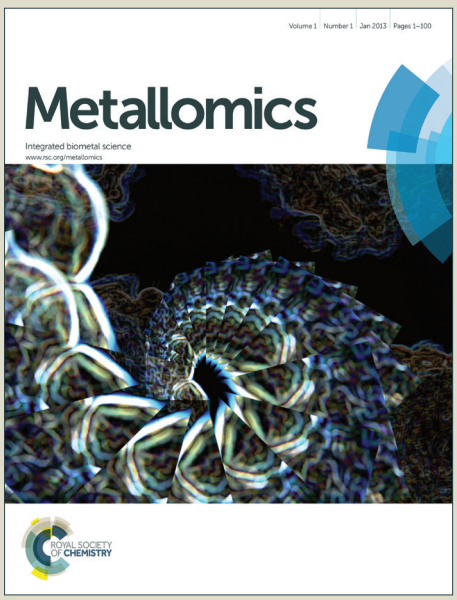

ROYAL SOCIETY OF CHEMISTRY

www.rsc.org/metallomics

Speciation of metal-based nanomaterials in human serum characterized by capillary electrophoresis coupled to ICP-MS: A case study of gold nanoparticles†

Magdalena Matczuk,[a] Karolina Anecka,[a] Federica Scaletti,[b] Luigi Messori,[b] Bernhard K. Keppler,[c] Andrei R. Timerbaev*[cd] and Maciej Jarosz[a]

[a] *Chair of Analytical Chemistry, Faculty of Chemistry, Warsaw University of Technology, Noakowskiego St. 3, 00-664 Warsaw, Poland*

[b] *Department of Chemistry "Ugo Schiff", University of Florence, Via della Lastruccia 3, 50019 Florence, Italy*

[c] *Institute of Inorganic Chemistry, University of Vienna, Waehringer Str. 42, A-1090, Vienna, Austria*

[d] *Vernadsky Institute of Geochemistry and Analytical Chemistry, Kosygin St. 19, 119991 Moscow, Russian Federation.*

E-mail: andrei.timerbaev@univie.ac.at; Fax: +7-495-938-2054; Tel: +7-495-939-7035

† Electronic supplementary information (ESI) available: Fig. S-1: electropherograms for gold nanoparticles of varying size. Fig. S-2: electropherograms of 5-nm gold particles interacting with albumin. Table S-1: binding of gold nanoparticles to transferrin. See DOI:

The development and optimization of a versatile analytical system for the speciation analysis of metal-containing nanoscale materials in blood serum is reported herein. Based on capillary electrophoresis (CE) interfaced with inductively coupled plasma mass spectrometry (ICP-MS), the method was shown feasible to investigate the interactions between serum proteins and gold nanoparticles of potential medicinal use, which are first and foremost occurrence upon their entering the circulatory system. To improve the separation resolution between the intact nanoparticles and different protein conjugates, the CE system was optimized with emphasis on compatibility with physiological conditions, avoiding aggregation effects, and analyte recovery. Optimization allowed also for acquiring the acceptable figures of merit such as migration time and peak area precision of 1.0–6.4% and 2.4–6.9%, respectively, detection limits in the range of 0.8–1.0 μg L^{-1} Au, and capillary recoveries on the order of 86–97%, depending on nanoparticle size and conjugate type. We sytematically investigated the role of size in mediating protein adsorption to gold nanoparticles in real-serum environment. At the initial stage of surface coating, the speciation of smaller particles (5 and 10 nm) was found to be dominated by albumin, transferrin (both in apo- and holo-form) playing the secondary role in developing the protein corona. For 20 and 50 nm nanoparticles, the contribution of transferrin is initially comparable; however, with time it becomes replaced by albumin. The time of attaining equilibrium adsorption is also a function of particle size but for the whole size range investigated, albumin is the only equilibrium binding partner. These principal findings prove that for metal-based nanomaterials in general, serum protein conjugates could be variable in composition in dependence to protein abundance and binding affinity, as well as the residence time in the bloodstream.

Introduction

Among various nanoscale materials that are intended for medicinal use, metal-based nanomaterials (MBNs) have gained perhaps the greatest attention in the last few years.[1,2] A wide range of new types of MBNs, having diagnostic or therapeutic functions (or both), continue to be created. Indispensably, each new MBN is to be evaluated with regard to issues of biocompatibility, toxicity, metabolism, distribution, cellular uptake, targeting, *etc*. before *in vivo* biomedical application. It is important to understand that regardless of the type and specific application, MBNs are administered intravenously. Therefore, blood circulatory system is a locus where the story of losing the original, synthetic identity and confronting biotransformations begins. Above all, interactions with plasma proteins give the MBN a new, biological identity[3] and thus significantly influence many properties and the biological response of MBN and dictate its behavior *in vivo*.[4–6]

Several analytical methods have been proposed for the characterization of MBN–protein interactions, identifying the contents of the protein corona formed on the MBN surface, and understanding the speciation alterations *in vivo*.[7,8] Of these methods, our choice here fell on capillary electrophoresis (CE) due to its proven record in biospeciation analysis.[9] Furthermore, as follows from a recent review in this journal,[10] the benefits of mild, species-friendly separation conditions, high degree of resolution, and acceptable tolerance to proteinaceous samples paved the way for CE as a direct probe to study the protein binding of MBNs, mostly nanoparticles. One of few disadvantages of CE in this application area, insufficient sensitivity, can be overcome by employing inductively coupled plasma mass spectrometry (ICP-MS) as detection method. Not only a highly sensitive and specific signal for many core/shell metals comprising MBNs, but also simultaneous monitoring of non-metals and often metals being a part of proteins is afforded by ICP-MS.[11–13]

Some of favorable analytical features of CE-ICP-MS were demonstrated in current research mostly focused on gold nanoparticles. Lin *et al*.[14] used gold nanoparticles as a tag to quantify albumin in human urine samples. Franze and Engelhard[15] and Qu *et al*.[16] adopted the combined method of interest for the characterization of dietary supplement products, containing as ingredients Au, Pt, and Pd nanoparticles. Most recently, Matczuk *et al*. have undertaken a study on assessing the quantitative performance of CE-ICP-MS.[17] A remarkable detection limit for gold nanoparticles of 2×10^{-15} M was attained after system optimization directed toward its application to biological samples.

With this in mind, we figured gold nanoparticles as a rational starting point for developing a fitting CE-ICP-MS methodology to systematically assaying the speciation of MBNs in human serum and possible alterations in speciation on the way from the point of administration to the cell. Another rationale behind the choice of gold nanoparticles was their commercial availability in a well characterized state and promise for multifunctional biomedical applications (multimodal diagnostic systems, targeted drug delivery, photothermal treatment of cancer).[18,19] While ICP-MS detection of Au presented no challenge, various factors were explored to maintain system compatibility with the protein-rich samples, preserve nanoparticle stability, and optimize the separation conditions. The developed method was first tested by using gold nanoparticle mixtures with individual serum proteins to demonstrate the accuracy and to enable identification of the protein conjugates in real samples. The recognition task was facilitated by simultaneous recording of ^{197}Au, ^{57}Fe, and ^{34}S isotopes. The method practicability was further established by analyzing nanoparticles of different (but distinct) size exposed to human serum *via ex vivo* incubation. The fact that the interaction of gold nanoparticles with proteins is a dynamic process, the particle size being a critical parameter affecting the composition of the protein corona, was attested by following the time-dependent changes in concentrations of free and protein-bound species of Au.

Experimental section

Chemicals and nanoparticle suspensions

Ultrapure Milli-Q water was obtained from a Millipore Elix 3 apparatus (Saint-Quentin, France) and used throughout. Gold nanoparticle suspensions (5, 10, 20, and 50 nm in nominal diameters) were acquired from British Biocell International (Cardiff, UK) and stored in darkness at 4 °C. The Au concentration in aqueous suspensions was characterized by the producer as 63.2, 57.6, 56.6 and 56.8 mg L^{-1}, respectively, that was confirmed by our ICP-MS measurements. All chemicals, protein standards (lyophilized powders, >97%), and human serum (from human male AB plasma), as well as three buffer types based on Na_2HPO_4–NaH_2PO_4, 4-(2-hydroxyethyl)piperazine-1-ethanesulfonic acid, or HEPES, and piperazine-N,N′-bis(2-ethanesulfonic acid), were purchased from Sigma-Aldrich (St. Louis, MO, USA).

Instrumentation

Analyses were performed on a HP^{3D}CE system (Agilent Technologies, Waldbronn, Germany) coupled to a 7500a ICP mass spectrometer (Agilent Technologies, Tokyo, Japan). Polyimide-coated fused-silica capillaries (i.d. 75 μm; o.d. 375 μm; length 70 cm) were obtained from CM Scientific Ltd. (Silsden, UK). The liquid-introduction interface was based on a model CEI-100 nebulizer (CETAC, Omaha, NE, USA) equipped with a low-volume spray chamber and a cross-piece to merge the sheath liquid flow. Electrical circuit of the CE was completed *via* a grounded platinum wire. Ten times diluted electrolyte buffer containing 20 μg L^{-1} Ge was used as the make-up solution. The mass isotopes of ^{197}Au, ^{57}Fe, and ^{34}S were monitored in order to observe the speciation changes upon binding of nanoparticles with serum proteins. The signal of ^{72}Ge was recorded to control the stability of hyphenation performance and the efficiency of nebulization. Instrumental control and data analysis were performed using Agilent ChemStation software. Operation conditions of the optimized CE-ICP-MS setup are summarized in Table 1.

A new capillary was initialized by flushing with 1 M NaOH for 30 min, followed by a 5-min rinse with water. The capillary was conditioned each day before use with 1 M NaOH for 15 min, water for 5 min, and running electrolyte for 15 min. Between each run, the capillary was purged with 1 M NaOH for 1.5 min, a mixture of 1 M NaOH, methanol, and water (25/50/25, v/v/v) for 1 min, water for 1 min and then equilibrated with the running electrolyte for 3 min. The temperature of the capillary cassette was set at 37 °C (physiological temperature). Samples were introduced by applying a 20 mbar pressure for a specified time. The applied voltage for carrying-out the separation was in the range 5–30 kV. The pH of running electrolyte was adjusted to 7.4 by adding 1 M NaOH. All solutions to be introduced into the capillary were filtered through 0.45 µm syringe filters (Millipore, France).

Sample preparation

Dilution of nanoparticle suspensions to the desired concentration was done with 10 mM phosphate buffer (pH 7.4) containing 100 mM NaCl. Concentration of the gold particles in all samples was adjusted to doses at which the therapeutic effect was observed during radiotherapy of mice tumors (1.35–2.7 g kg^{-1} Au).[20] Using a recalculation factor that takes into account an average mass of human body, the volume of blood, the percentage of serum in blood, and sample dilution factor (1000- or 2000-times), the final concentration of

nanoparticles in mixtures with individual proteins or in serum samples was set in the range of 9.5–38 mg L^{-1} Au.

An aliquot of gold nanoparticle stock solution was added to individual protein solution in 10 mM phosphate buffer (pH 7.4) containing 100 mM NaCl (final concentration of albumin or transferrin 19 and 3 mg L^{-1}, respectively). The mixture was incubated for a maximum of 24 h at 37 °C to allow protein adsorption prior to sample introduction into the CE-ICP-MS system. The samples of gold nanoparticles mixed with 1000-times diluted human serum were incubated and analyzed as before. None of the preparations showed visible signs of particle aggregation.

Results and discussion

Optimization of CE conditions

In order to enhance the separation efficiency and attain quantitative elution of nanoparticles and their protein conjugates from the separation capillary, several electrophoretic buffers were evaluated. Although previous studies have suggested that increasing the pH of the background electrolyte improves the migration behavior of nanoparticles (by virtue of a greater electrostatic repulsion from negatively charged capillary walls),[10] the preference was given to the buffers with marked buffering capacity around the physiological pH, *i.e.* pH 7.4. As a rule of thumb, working at this pH would secure the conjugates formed under simulated or real physiological conditions from pH-induced changes in the CE system. Also for the reason of compatibility with incubation settings, the use of surfactants was avoided in this study. Adding a charged surfactant to the running electrolyte is known as a factor contributing to an improved separation of differently sized gold nanoparticles;[15,16,21,22] however, this was beyond our present goals.

Of three tested buffers systems capable to provide essentially neutral conditions (as detailed in the Experimental section), HEPES was found to be the most suitable as affording the highest signals of analytes under scrutiny as well as superior separation conditions with respect to peak shape and migration times. The effect of the HEPES concentration was examined in the range of 10–40 mM. Results showed that a concentration of 40 mM represents an optimum for separation of target analytes, including early migrating species originating from serum (the transferrin conjugates). Also, the baseline noises attributed to

high sample conductivity (100 mM chloride) appear to be smaller with 40 mM HEPES. Accordingly, 40 mM HEPES, pH 7.4 was chosen for baseline separation of gold particles and particle–protein conjugates.

The next operational parameter optimized was the applied voltage, affecting mostly the migration times. Higher voltages produced less broadened peaks over a shorter time frame, and 15 kV (generating a current of 14 μA) was found to be optimal. Measurements using voltage ≥20 kV resulted in poorly resolved electropherograms. In its turn, sample loading was varying with the aim of gaining the highest signals without sacrificing capillary recovery and peak efficiency. It was noticed, however, that the loading is limited by the adsorption of excessive proteins in the sample, as well as the protein conjugates, on capillary walls, leading to less reproducible migration times and current instability. Therefore, increasing the loading above 100 mbar×s was considered unreasonable. Consequently, the experiments described below were performed with the separation voltage of 15 kV and sample loading at 20 mbar for 5 s.

From electropherograms shown in Figure S-1 (ESI†), it can be seen that with the optimized parameters all gold nanoparticles under investigation exhibit a symmetrical signal, the peak efficiency being slightly compromised upon increasing the particle diameter. While smaller particles migrate definitely slower, the particle size showed a moderate effect on the migration time (see Figure S-1). As displayed below, the formation of the protein corona, though considerably increasing the size of gold nanoparticles, did not affect notably peak symmetry. Presented in Table 2 are analytical figures of merit of the developed CE-ICP-MS assay. Results indicate a good precision of the method, with relative standard deviations of peak areas of 2.4–5.5% and 3.8–6.9% for intraday (n = 6) and interday (n = 3) measurements, respectively. Migration time precision was typically below 3% that is the customary level in CE. In contrast to previously published studies on gold nanoparticles,[23,24] no influence of the particle size on detection sensitivity was observed here. Detection limits slightly varied, from 0.8 to 0.9 μg L^{-1} Au, for a given set of nanoparticles. Their transformation into the albumin-bound form exerted negligible effect on sensitivity. These observations prove complete vaporization and ionization of the Au species of interest in the ICP, independent of their size and chemical nature. On the other hand, capillary recoveries assessed by comparison of the results acquired in electrophoretic and pressure-driven modes, being almost identical and quantitative for 5-, 10-, and 20-nm-sized particles, decreased in the case of 50 nm nanoparticles to approximately 87%. Note that analyte mass loss witnessed in the current study is considerably lower than in other capillary-based separation techniques (*cf.* recoveries

of 72–80% for gold nanoparticles of the same diameters in micellar electrokinetic chromatograhy[15]). The effect of particle size on the recovery was yet more pronounced for respective albumin conjugates (see Table 2). This can be attributed to a greater tendency to adsorb onto capillary walls for larger proteinaceous nanostructures.

Interaction with individual proteins

Binding of gold nanoparticles to plasma proteins is known to proceed with fast kinetics.[14,25,26] For albumin, rapid formation of the protein corona was clearly seen in our experiments: after 5 min of incubation no peak of free 10–50 nm nanoparticles in mixtures (at eventually therapeutic concentration ratio) was recorded due to complete conversion into the protein-covered form. It is important to mention that the molar excess of albumin was about 180, 1500, and 23000 for 10-, 20-, and 50-nm sized particles, respectively. Increasing the nanoparticle concentration from 9.5 to 19 mg L^{-1} Au (still within the therapeutic range) displayed no visible effect on binding rate. Association with albumin decreased the electrophoretic mobility of nanoparticles in line with increasing their size, while the accompanying change in the surface charge seems to have lower effect. Consequently, the migration times toward the anode placed at the detection side of the capillary (counter-electroosmotic flow mode) were shortened.

The fact that nanoparticle size is a critical parameter affecting the protein conjugation was only evidenced when the smallest, 5-nm particles were subject to examination. With merely 20-fold molar excess of albumin, the evolution of the conjugate formation proceeds markedly slower. This allowed for recording the peak belonging to the naked nanoparticles (at about 13 min) at incubation times up to 48 min (Figure S-2; ESI†). Applying a twofold concentration of gold particles, *i.e.* 2.5×10^{-8} M (corresponding to a dose of 2.7 g kg^{-1} Au), led to further deceleration of albumin binding. As a result, even after 24 h of incubation, 5% of nanoparticles remained in unbound state. This observation has certain biological implication from the standpoint of cellular uptake of gold nanoparticles, given, in particular, that smaller sizes favor better targeting specificity.[27]

From a linear relationship between relative peak area of 5 nm gold particles and incubation time (regarded up to 30 min), presented in Figure 1, the apparent rate constant was calculated as 1.56×10^{-3} min^{-1}. However, this value can be used only for comparative reasons, as in fact interaction with albumin is far from being simple, first-order reaction. At the initial stage (1–5 min), the development of binding is very fast, resulting in about 95% of

nanoparticles covered with protein molecules. Thereafter the binding reaction slows down, thus showing an apparent two-step character. We attribute such binding pattern to the mechanism underlying time-related changes in the structure of albumin after adsorption on gold nanoparticles. The protein adsorption is due to at least two driving forces, electrostatic interaction[28] and sulfur–gold bonding.[29] The electrostatic interaction occurs immediately, but the covalent interaction between Au in nanoparticles and S in albumin takes a longer time and induces distinctive structural changes of the protein.[30] As a matter of fact, a stepwise character of nanoparticle proteinization could be true for the whole size range under investigation. However, the CE method in use is not suitable for assessing very fast reactions.

Transferrin exists in human blood in two forms: iron-free or apo-transferrin (about 70%) and iron-saturated, holo-transferrin, amounting *ca*. 30%.[31] Strikingly, interaction of the gold nanoparticles with the physiological mixture of transferrin forms brought about the development of two types of conjugates (an assumption of which was formerly made[32]). As can be seen in Figure 2, an early migrating peak is due to binding to holo-transferrin, which takes place without iron replacement (see the supplementary ^{57}Fe-trace). In its turn, the sulfur-specific electropherogram serves as a clue of proteinaceous nature of the respective peaks (we gave the preference to the ^{34}S isotope over much more abundant ^{32}S for the reason of circumventing the spectral interferences due to oxygen). Evidently, because of the protein coating, enclosing the iron atoms, a net negative charge of the holo-transferrin conjugate is smaller than that of the apo-transferrin one (but the size is similar). Such charge-to-size difference explains the migration order observed. Another observation in favor of peak assignment in Figure 2 is that the ratio of peak areas of two conjugates matches the percentage of transferrin forms in original mixture.

As in the case of albumin, the transferrin binding is a fast process, with equilibrium being reached in about 5 min, after which no further increase in conjugates peak areas was visible. However, on contrary, the equilibrium speciation of Au (see Figure 2, lower trace) is dominated by uncovered (instead of covered) nanoparticles. Results shown in Table S-1 (ESI†) indicate that the formation of both transferrin conjugates intensifies with particle size. Nonetheless, even with the largest particles (50 nm), the total amount of conjugates is only about 10%. On the opposite side of the size range, for 5 nm nanoparticles, no conjugates were detectable.

Speciation in human serum

In real biological systems, nanoparticles encounter proteomes, not a single protein. This implies that in case of human serum, the protein corona could be a temporarily dynamic complex whose formation and composition is governed by protein abundance and binding affinity.[33,34] Figure 3 shows typical protein-binding profiles acquired for 20 nm gold nanoparticles exposed to human serum for a different period of time. It is worthwhile noting that whereas the accommodation of three proteins on the nanoparticle surface is evidenced using CE-ICP-MS, the actual number of the serum-protein conjugates might be greater.[35] However, their abundances are much lower, thus falling beyond the limit of detection. A detailed look into the speciation pattern recorded revealed that after 2 min, which is a possible temporal situation after intravenous injection, nanoparticles lose their identity being in comparable proportions transformed into albumin and transferrin conjugates. It is important to point out that when a standard mixture of all three proteins involved in coating (at their physiological concentrations) was used instead of serum, the results were totally different: regardless of the particle size, only albumin participated in forming the corona. We ascribe this dissimilarity to surface modification by serum matrix components that could change the affinity of gold nanoparticles toward different proteins.

With time, both forms of transferrin adsorbed on the particle surface tend to be replaced by albumin that turns to be the only constituent of the protein corona when it reaches an equilibrium state. According to our measurements (see Figure 3), for this size of particles such a state becomes due in 4 h which is equivalent of prolonged circulation in the blood. It is also evident that under real-world conditions, binding to albumin is kinetically less favorable. This is manifested by evident peak tailing until the conjugate formation is completed. After 4 h, no further alterations in the speciation of Au were seen and the albumin conjugate remained stable for at least 24 h.

There are several conclusions that can be inferred from the observed binding scenario. First, surface coating is a collective and dynamic process whereby serum proteins are adsorbed in a competitive manner. Second, the selectivity in protein binding is influenced by the properties of the proteins, both albumin and transferrin showing apparently a comparable affinity to the surface of nanoparticles. However, in the long run, a higher abundance of albumin prevails. Finally, the albumin conjugate serves most likely as the form in which the gold nanoparticles accumulate within the tumor and reach the desired cells.

Similar speciation profiles were obtained for gold particles of other sizes. While their conversion into the protein-bound forms was similar in speed, the size of nanoparticles exerted an impact on the mechanism of protein binding. It is evident that the larger the

diameter, the greater is the percentage of the transferrin conjugates at the initial, reversible step of proteinization (Table 3). Also time required to attain the equilibrium binding (in all cases, to albumin) increases with growing the particle diameter. Another analyte characteristic which is a function of size is capillary recovery, measuring up in all cases a satisfactory level well above 80%.

Summarizing, our study demonstrated that even within a single class of gold nanoparticles with identical surface capping, their behavior following exposure to human serum is fairly diverse. Depending on the size and residence time, the protein corona varies in composition which may have fundamental biological consequences.

Conclusions

Whatever the biomedical implications can be made from the current study, we consider its main outcome in developing a multipurpose analytical platform to analyze MBN–protein interactions. Therefore, it is safe to assume that with the same or slightly modified basic setup, the CE-ICP-MS can be applied to other MBNs, different in the core/shell metals, shape and size, or surface chemistry. Due to high-resolution CE separation and ultrasensitive ICP-MS detection the methodology presented herein has potential for a highly efficient monitoring and comprehensive understanding of the interactions of nanoparticles with their binding partners, including the cytoplasmic components of cells, which is crucial for their implementation into the clinical setting.

Acknowledgements

Financial support provided by the National Science Centre in Poland (PRELUDIUM, grant no. 2013/11/N/ST4/01480) is gratefully acknowledged.

References

1 H.-C. Huang, S. Barua, G. Sharma, S. K. Dey and K. Rege, *J. Controlled Release*, 2011, **155**, 344–357.

2 E.-K. Lim, T. Kim, S. Pail, S. Haam, Y.-M. Huh and K. Lee, *Chem. Rev.*, 2015, **115**, 327–394.

3 M. P. Monopoli, C. Åberg, A. Salvati and K. A. Dawson, *Nature Nanotechnol.*, 2012, **7**, 779–786.

4 B. Wang, W. Feng, Y. Zhao and Z. Chai, *Metallomics*, 2013, **5**, 793–803.

5 Q. Mu, G. Jiang, L. Chen, H. Zhou, D. Fourches, A. Tropsha and B. Yan, *Chem. Rev.*, 2014, **114**, 7740–7781.

6 J. Lazarovits, Y. Y. Chen, E. A. Sykes and W. C. W. Chan, *Chem. Commun.*, 2015, **51**, 2756–2767.

7 Z. W. Lai, Y. Yan, F. Caruso and E. C. Nice, *ACS Nano*, 2012, **6**, 10438–10448.

8 A. L. Capriotti, G. Caracciolo, C. Cavaliere, V. Colapicchioni, S. Piovesana, D. Pozzi and A. Laganà, *Chromatographia*, 2014, **77**, 755–769.

9 A. R. Timerbaev, *Chem. Rev.*, 2013, **113**, 778–812.

10 S. S. Aleksenko, A. Y. Shmykov, S. Oszwałdowski and A. R. Timerbaev, *Metallomics*, 2012, **4**, 1141–1148.

11 P. Krystek, A. Ulrich, C. C. Garcia, S. Manohar and R. Ritsema, *J. Anal. At. Spectrom.*, 2011, **26**, 1701–1721.

12 A. R. Montoro Bustos, J. R. Encinar and A. Sanz-Medel, *Anal. Bioanal. Chem.*, 2013, **405**, 5637–5643.

13 A. R. Timerbaev, *J. Anal. At. Spectrom.*, 2014, **29**, 1058–1072.

14 J.-M. Lin, Y. Li, Y. Jiang and X.-P. Yan, *J. Proteome Res.*, 2010, **9**, 3545–3550.

15 B. Franze and C. Engelhard, *Anal. Chem.*, 2014, **86**, 5713–5720.

16 H. Qu, T. K. Mudalige and S. W. Linder, *Anal. Chem.*, 2014, **86**, 11620−11627.

17 M. Matczuk, S. S. Aleksenko, F.-M. Matysik, M. Jarosz and A. R. Timerbaev, *Electrophoresis,* 2015, **36**, 1158–1163.

18 P.-F. Jiao, H.-Y. Zhou, L.-X. Chen and B. Yan, *Curr. Med. Chem.*, 2011, **18**, 2086–2102.

19 J.-J. Liang, Y.-Y. Zhou, J. Wu and Y. Ding, *Curr. Drug Metabol.*, 2014, **15**, 620–631.

20 J. F. Hainfeld, D. N. Slatkin and H. M Smilowitz, *Phys. Med. Biol.*, 2004, **49**, N309–N315.

21 F.-K. Liu, *J. Chromatogr. A*, 2009, **1216**, 2554–2559.

22 F.-K. Liu, *Anal. Sci.*, 2010, **26**, 1145–1150.

23 J. W. Olesik and P. J. Gray, *J. Anal. At. Spectrom*., 2012, **27**, 1143–1155.

24 K.-S. Ho, K.-O. Lui, K.-H. Lee and W.-T. Chan, *Spectrochim. Acta, Part B*, 2013, **89**, 30–39.

25 N. Li, S. Zeng, L. He and W. Zhong, *Anal. Chem.*, 2010, **82**, 7460–7466.

26 M.-Y. Xie, Z.-P. Guo and Y. Chen, *Chem. J. Chin. Univ.*, 2010, **31**, 2162–2166.

27 J. Wang, R. Bai, R. Yang, J. Liu, J. Tang, Y. Liu, J. Li, Z. Chai and C. Chen, *Metallomics*, 2015, **7**, 516–524.

28 S. H. Brewer, W. R. Glomm, M. C. Johnson, M. K. Knag and S. Franzen, *Langmuir*, 2005, **21**, 9303–9307.

29 S. Chakraborti, P. Joshi, D. Chakravarty, V. Shanker, Z. A. Ansari, S. P. Singh and P. Chakrabarti, *Langmuir*, 2012, **28**, 11142–11152.

30 C. Fu, H. Yang, M. Wang, H. Xiong and S. Yu, *Chem. Commun*., 2015, **51**, 3634–3636.

31 P. T. Gomme, K. B. McCann and J. Bertolini, *Drug Discov. Today*, 2005, **10**, 267–273.

32 P.-H. Yang, X. Sun, J.-F. Chiu, H. Sun and Q.-Y. He, *Bioconjugate Chem.*, 2005, **16**, 494–496.

33 E. Casals, T. Pfaller, A. Duschl, G. J. Oostingh and V. Puntes, *ACS Nano*, 2010, **4**, 3623–3632.

34 M. Lindquist, J. Stigler, T. Cedervall, T. Berggard, M. B. Flanagan, I. Lynch, G. Elia and K. A. Dawson, *ACS Nano*, 2011, **5**, 7503–7509.

35 C. D. Walkey, J. B. Olsen, H. Guo, A. Emili and W. C. W. Chan, *J. Am. Chem. Soc*., 2012, **134**, 2139−2147.

Table 1 CE-ICP-MS operating parameters

CE system	
Capillary	fused silica capillary, I.D. 75 μm, O.D. 375 μm, length 70 cm
Capillary electrolyte	HEPES 40 mM, pH 7.4
Voltage	15 kV
Temperature	37 °C
Sample injection	hydrodynamic, 20 mbar, 5 s
ICP-MS system	
RF power	1320 W
Sample depth	6.7 mm
Plasma gas	15.0 L min^{-1}
Nebulizer gas flow	1.1 L min^{-1}
Monitored isotopes	^{197}Au, ^{57}Fe, ^{34}S, ^{72}Ge

Table 2 Precision, detection limits and capillary recovery

Species[a]	RSD (%)				Detection limit (μg L^{-1} Au)[b]	Capillary recovery (%) (n = 6)
	Migration time		Peak area			
	Intraday (n = 6)	Inter-day (n = 3)	Intraday (n = 6)	Inter-day (n = 3)		
Gold nanoparticles (nm)						
5	1.5	2.2	3.9	4.2	8.2	96.8±0.5
10	1.4	1.8	3.6	3.9	8.3	96.6±0.5
20	1.3	1.4	3.6	3.8	8.5	96.3±0.5
50	2.5	2.8	5.5	6.5	9.2	93.5±0.3
Gold nanoparticle (nm)–albumin conjugate						
5	1.0	2.1	2.4	4.2	8.3	95.7±0.2
10	2.6	3.7	2.6	4.0	8.5	95.3±0.3
20	3.6	5.6	4.3	4.5	8.8	92.7±0.5
50	4.1	6.4	4.9	6.9	9.9	86.8±0.6

[a] 9.5 mg L^{-1} Au alone or after 1-h incubation with 19 mg L^{-1} albumin. [b] 3σ criterion.

Table 3 Protein-mediated transformations of gold nanoparticles in human serum

Size (nm)	Relative peak area (%)[a]			Equilibrium time (h)[b]	Capillary recovery (%)[c]
	Holo-transferrin	Apo-transferrin	Albumin		
5	0.8±0.1	1.4±0.1	97.8±0.1	0.3	91.3±0.2
10	7.2±0.1	8.0±0.1	84.8±0.1	1	90.2±0.2
20	16.5±0.2	19.5±0.1	64.0±0.2	4	88.8.±0.3
50	21.6±0.3	25.3±0.3	53.1±0.5	24	83.5±0.3

[a] Analyses after 2 min of sample incubation; $n = 3$. [b] Time at which relative peak area of the albumin conjugate attains 100%. [c] Calculated on the basis of measurements made after 30-min incubation; $n = 3$.

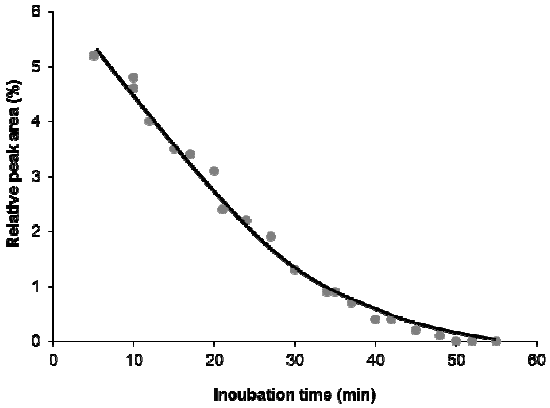

Fig. 1 Dependence of nanoparticle signal on the time spent on coating with albumin. The relative peak area was calculated as the ratio of the peak area of bare 5-nm nanoparticles to the total area of peaks due to uncoated and coated particles. For conditions, see Table 1 and Experimental section.

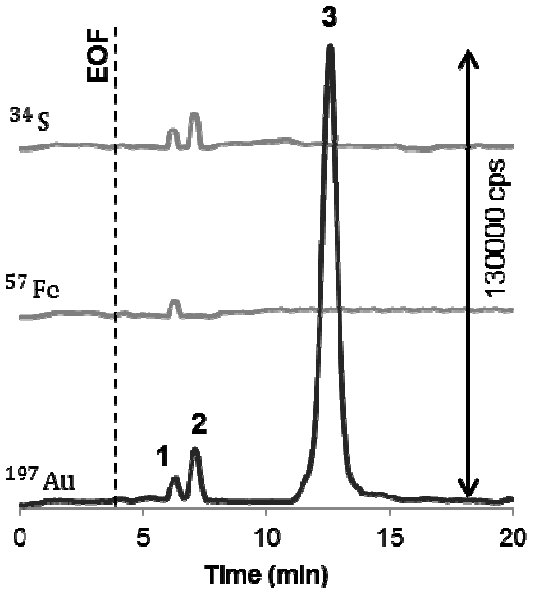

Fig. 2 Electropherograms illustrating the progress in conjugation between 20-nm gold particles and transferrin after 30 min. Sample: 19 mg L^{-1} gold nanoparticles, 3 mg L^{-1} transferrin in 10 mM phosphate buffer (pH 7.4), 100 mM NaCl. Peak assignment: 1 – holo-transferrin conjugate; 2 – apo-transferrin conjugate; 3 – gold nanoparticles. See Table 1 and Experimental section for CE-ICP-MS conditions.

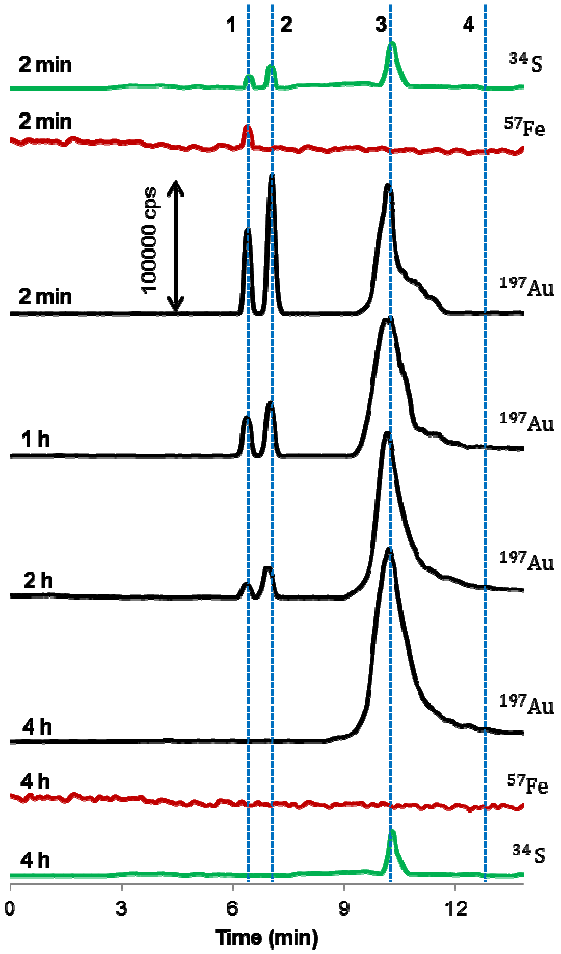

Fig. 3 Time-dependent speciation of 20-nm gold particles in human serum. Sample: 19 mg L^{-1} gold nanoparticles in 1000-times diluted serum. Peak assignment: 1 – holo-transferrin conjugate; 2 – apo-transferrin conjugate; 3 – albumin conjugate. Line 4 shows the migration time of intact nanoparticles. See Table 1 and Experimental section for CE-ICP-MS conditions.